Eklund, Amanda; Hu, Shanming; Fang, Yuhuang; Savolainen, Henri; Pi, Haotian; Zeng, Hao; Priimagi, Arri; Ikkala, Olli; Zhang, Hang

Bright and Switchable Whiteness in Macro-Crosslinked Hydrogels

Published in:
ADVANCED OPTICAL MATERIALS

DOI:
10.1002/adom.202302487

Published: 15/04/2024

Document Version
Publisher's PDF, also known as Version of record

Please cite the original version:
Eklund, A., Hu, S., Fang, Y., Savolainen, H., Pi, H., Zeng, H., Priimagi, A., Ikkala, O., & Zhang, H. (2024). Bright and Switchable Whiteness in Macro-Crosslinked Hydrogels. *ADVANCED OPTICAL MATERIALS*, *12*(11), Article 2302487. https://doi.org/10.1002/adom.202302487

ADVANCED OPTICAL MATERIALS
www.advopticalmat.de

Bright and Switchable Whiteness in Macro-Crosslinked Hydrogels

*Amanda Eklund, Shanming Hu, Yuhuang Fang, Henri Savolainen, Haotian Pi, Hao Zeng, Arri Priimagi, Olli Ikkala, and Hang Zhang**

Bright white color is often achieved in nature by the combination of polydisperse scattering structures and high refractive index contrast between the scatterer and the surrounding medium. Similarly, synthetic systems have commonly utilized inorganic materials as the scattering centers to achieve white color, which, however, lacks the ability to switch the optical properties. While hydrogels capable of scattering light are utilized in applications such as smart windows, their reflection properties have remained limited due to the low refractive index contrast between the polymer and water. As a result, thick layers in the millimeter range are often required to achieve reasonable whiteness. Here a hydrogel consisting of a temperature-responsive poly(*N*-isopropylacrylamide) (PNIPAm) and chemically modified agarose used as a chemical macro-crosslinker is presented. The hydrogel exhibits high whiteness at temperatures above the phase transition (≈31 °C). The reflectance at 800 nm is four times as high as for standard PNIPAm, and a change in transmittance can be induced by laser pulses as short as 30 ms. The macro-crosslinked structure of this hydrogel provides superior reflectance at a lower thickness compared to reported hydrogel systems, enabling a variety of potential applications including smart windows, responsive displays, optical switches, and camouflage.

1. Introduction

Bright whiteness in materials has gained growing interest due to the widespread potential applications in fields ranging from paints,[1] food,[1,2] and cosmetics[1,2] to screens,[3] radiative cooling,[4] and smart windows.[5] A white appearance is a result of the materials' ability to evenly scatter all wavelengths of visible light.[6,7] This property is influenced by the optical thickness of the material,[7–9] the refractive index difference at the scattering interfaces[8] as well as the material morphology.[6,9] Generally, white materials have an anisotropic, disordered structure, which leads to multiple light scattering.[8–12]

To achieve maximal whiteness, traditional synthetic systems have relied on approaches maximizing the refractive index difference between the material constituents such as utilizing TiO_2, which has a high refractive index of ≈2.6.[2,13] In natural systems consisting of polymers with a relatively low refractive index of ≈1.5, white appearance is generally achieved by photonic structures that maximize light scattering.[6,8,11,14,15] Several synthetic systems have been developed that mimic these porous structures and provide high whiteness even at low thicknesses.[1,7,16,17] However, the optical properties of these systems tend to either be static, or lack sufficient refractive index contrast to remain white when submerged in water.[8,16]

Using stimuli-responsive hydrogels that undergo phase separation under certain conditions has led to advances in improving the scattering properties in hydrogel systems and polymer solutions.[18] Both hydroxypropyl cellulose[19–23] (HPC) and poly(*N*-isopropylacrylamide)[3,23–25] (PNIPAm) are often used in such contexts as they become opaque upon heating due to phase transitions in solubility.[5,26] Commonly these systems are optimized for use in smart windows to regulate the indoor temperature and reduce the amount of energy used for cooling by blocking sunlight as temperature is increased above the transition temperature.[5,27–30] Some systems are also designed to function as privacy windows during the night at lower temperature.[31] However, due to the relatively low polymer content and low refractive index contrast to water, higher thicknesses are generally required in these systems compared to static dry materials.[9]

In this work, we present macro-crosslinked (MCL) PNIPAm hydrogels based on chemically modified agarose. The hydrogels exhibit a high whiteness above their phase transition temperature at ≈31 °C, and high transparency at room temperature (RT). This is achieved even at thicknesses commonly used in dry materials as a result of an optimal pore size distribution in the phase

A. Eklund, S. Hu, Y. Fang, H. Savolainen, H. Pi, O. Ikkala, H. Zhang
Department of Applied Physics
Aalto University
Espoo 02150, Finland
E-mail: hang.zhang@aalto.fi

H. Zeng, A. Priimagi
Faculty of Engineering and Natural Sciences
Tampere University
Tampere 33101, Finland

The ORCID identification number(s) for the author(s) of this article can be found under https://doi.org/10.1002/adom.202302487

DOI: 10.1002/adom.202302487

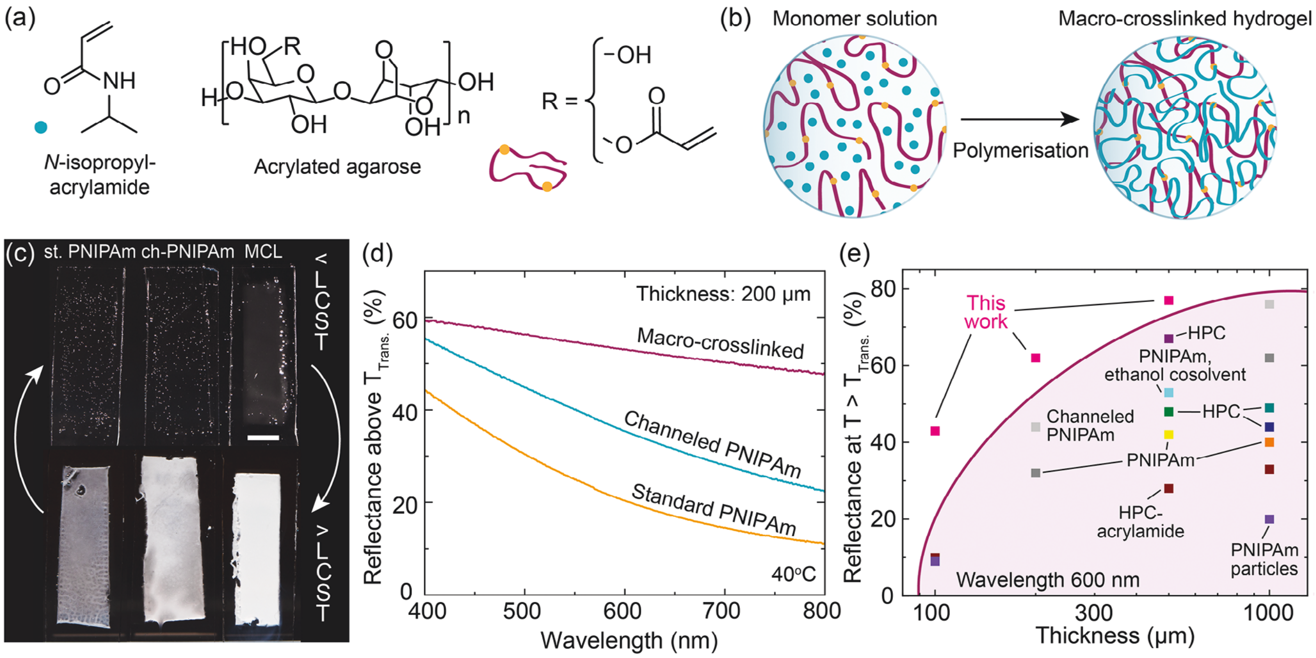

Figure 1. Bright whiteness in macro-crosslinked hydrogels. a) Chemical composition of monomer *N*-isopropylacrylamide and the chemical crosslinker acrylated agarose. b) Illustration of the polymerization process from a monomer solution to the macro-crosslinked hydrogel. c) Photographs of 200 µm thick films of st. PNIPAm, ch-PNIPAm, and MCL PNIPAm hydrogel, showing the switching between the transparent state below the LCST) and the white state above the LCST. d) Reflectance spectra of 200 µm thick film of MCL, ch-PNIPAm, and st. PNIPAm at 40 °C. The MCL hydrogel contained 15 wt.% NIPAm and 1 wt.% of acrylated agarose with an acrylation degree of 15%. Both ch-PNIPAm and st. PNIPAm contained 10 wt.% of NIPAm, and 0.1 mol.% of *N,N'*-methylenebisacrylamide as a crosslinker. 0.3 wt.% of agarose was used in the preparation of ch-PNIPAm. e) Comparison of the MCL reflectance at 600 nm to previously published polymer-water systems based on PNIPAm and HPC. Full references can be found in Figure S1a and Table S1 (Supporting Information).

separated state, which can be attributed to the larger and more polydisperse pores using the agarose as the macro-crosslinker compared to standard PNIPAm. Both the hydrogel reflectance and the switching ability are improved when compared to previously reported switchable hydrogel and polymer solution systems. This allows applications ranging from controllable reflecting screens,[3] deformable and optically switchable films, to optical switches.[32]

Table 1. CIELAB coordinates of the 200 µm thick hydrogel films.

Sample	L* [lightness, 0–100]	a* [green–red]	b* [blue–yellow]
MCL	78.7	−0.71	−3.3
ch-PNIPAm[3]	69.1	−2.4	−11.4
st. PNIPAm	56.7	−2.0	−17.3

2. Results and Discussion

2.1. Switching of Bright Whiteness in a Macro-Crosslinked Hydrogel

The MCL hydrogel is prepared using acrylated agarose as the chemical crosslinker in a temperature-responsive PNIPAm network. All components, shown in **Figure 1a**, are dissolved in water and polymerized at 45 °C using UV-initiated free radical polymerization,[33,34] which is above the gelation point of agarose and the lower critical solution temperature (LCST) of the PNIPAm. An illustration of the resulting network structure is shown in Figure 1b. The structure enhances the hydrogel reflectance above the LCST compared to standard PNIPAm (st. PNIPAm), as well as to a previously reported brightly white channeled PNIPAm (ch-PNIPAm) hydrogel.[3] This improvement can be seen in the photographs in Figure 1c and the reflectance spectra in Figure 1d. While the MCL hydrogel shows a reflectance between 60% and 47% across the visible wavelength spectrum at a thickness of 200 µm, the reflectance of ch-PNIPAm is between 55% and 20%, and the st. PNIPAm between 45% and 10%. The ch-PNIPAm and st. PNIPAm also have a blue hue due to higher reflectance in the smaller wavelength range compared to the longer wavelengths, while the MCL hydrogel exhibits uniform whiteness. The difference in reflective properties between these hydrogels was further studied by calculating their CIELAB coordinates, which are presented in **Table 1**. For a perfectly white materials the lightness $L^* = 100$, and the other coordinates that define hue, a^* and b^*, are close to zero.[35] It can be seen that the MCL hydrogel has a higher lightness while also being less green or blue in its hue compared to both ch-PNIPAm and st. PNIPAm.

Figure 1e compares the MCL hydrogel with previously reported hydrogel and polymer solution systems. The MCL hydrogel shows significantly improved thickness-dependent reflectance. The full references for the figure are presented in Figure S1a and Table S1 (Supporting Information). The water-containing hydrogel and polymer solution systems are based on PNIPAm[3,23–25] and HPC.[19–23] The reported systems have typical thicknesses between 100 and 10 000 µm with the highest reflectance at 600 nm shown by 1 mm thick ch-PNIPAm at 76%.[3] The MCL shows similar reflectance of 77% at the thickness of only 500 µm. On the other hand, the HPC solution presented by Connelly et al.[19] shows reflectance of 67% at the thickness of 500 µm, ≈10% less than the MCL hydrogel at the same thickness.

In Figure S1a (Supporting Information), non-aqueous systems are also presented for comparison. In the figure, insect scales are shown as reference materials in the top left corner of the figure, which provides extremely high reflectance at small thicknesses due to the higher refractive index contrast in such systems. Most of the dry materials consist of foam or dry polymer network structures, such as the cellulose-based nanocellulose fibril films,[13] and the bio-inspired cellulose acetate structure.[17] Different materials, such as fluoropolymers[7] and polyvinyl alcohol,[36] and processing methods, such as carbon dioxide foaming[1] and phase separation[16] of poly(methyl methacrylate) are used to maximize the whiteness in these thin structures. The dependence of reflectance on the thickness of reflecting layer can be seen as the reflectance increase from ≈60% to 99% as the layer thickness increases from 10 to 300 µm.

2.2. Influence of Hydrogel Composition on the Light Reflectance

The effect of the different compositions on the hydrogel reflectance is presented in **Figure 2**. The hydrogels were chemically attached between two silanized glass slides using parafilm as spacer to prevent dehydration and shrinking during measurement. A control sample containing only water instead of hydrogel is shown in the figure to estimate contribution to reflectance. The effect of monomer concentration is presented in Figure 2a–c. It can be seen that the highest reflectance of 67% at 400 nm can be reached when using 15 wt.% of NIPAm, whereas both 10 and 20 wt.% of the monomer result in a lower reflectance. Highest switching between the two reflectance states, ΔReflectance = 60%, is also reached using the 15 wt.% monomer concentration.

On the other hand, agarose concentration does not have a large effect on hydrogel reflectance as is shown in Figures 2d–f. While hydrogels containing either 1 or 1.5 wt.% of agarose reach 67% reflectance at 400 nm, the 1 wt.% of agarose results in slightly higher reflectance compared to the other concentrations at 600 and 800 nm. Similar trend is also seen in reflectance switching, as lower concentrations of agarose results in the higher reflectance.

Figure 2g–i show the effect of the acrylation degree of agarose on hydrogel reflectance. The degree of acrylation refers to the feed ratio of the acryloyl chloride to the available hydroxymethyl groups in agarose during acrylation process. The ^{1}H-NMR spectra of acrylated agarose and degree of substitution calculated from NMR spectra are shown in Figure S2 and Table S2 (Supporting Information), respectively. In this manuscript, degree of acrylation is used for consistency due to large errors of degree of substitution at low feed ratios. At all wavelengths, 15% acrylation degree results in the highest reflectance with the maximum at 67% at 400 nm. The second highest reflectance (56–65%) can be reached using 10% acrylation, while samples prepared using either 30 or 50% acrylation have a lower reflectance (between 50–65% and 47–62%, respectively). The effect of different acrylation degrees on the reflectance switching is similar but the difference between samples is more pronounced.

The effect of agarose type on reflectance is studied in Figure S3 (Supporting Information). It can be seen that the type of agarose also affects the reflectance in the gel, which differ in their chemical composition, melting point, network structure, and gel strength. Overall, the agarose A3 shows one of the highest reflectance compared to other types of agarose, while being easily processable due to its moderate melting point at 63 °C. Therefore, A3 is used throughout this manuscript.

As is common with scattering materials, the thickness of the reflecting layer plays a very large role in the resulting reflectance as can be seen in **Figure 3**a–c. The highest reflectance of 76% is reached with the 500 µm thick sample. Figure S1b (Supporting Information) presents the difference between the high and low reflectance states as a function of material thickness for different material systems. Full references can be found in Figure S1 and Table S1 (Supporting Information). The MCL hydrogels also demonstrate highest switching in reflectance at the presented thicknesses compared to reported systems.

2.3. Characterization of Hydrogel Microstructure

The hydrogel porosity is studied in more detail to determine the correlation between the microscopic structure and the high whiteness. The microstructure is analyzed by scanning electron microscopy of freeze-fractured and lyophilized hydrogels in liquid nitrogen after equilibration at RT or at 60 °C. At 60 °C, the MCL hydrogel has the same reflectance as at 40 or 50 °C (Figure S4, Supporting Information), indicating unchanged microscopic structures. 60 °C was therefore used to prevent the MCL hydrogel from transitioning back to transparent state during the preparation process for lyophilization. SEM images of the freeze-dried st. PNIPAm and MCL hydrogel are presented in **Figure 4**a,b,d,e, respectively. The pore densities, i.e., the number of pores of a certain diameter per unit area in the SEM images, are presented in Figure 4c,f. For st. PNIPAm the pore density maximum is reached at RT, while in the case of the MCL hydrogel, the largest pore density is detected at 60 °C. The decreased pore density of st. PNIPAm at high temperature is due to the phase separation leading to the collapse of dissolved polymer chains into hydrophobic domains.[3,26,37]

In the case of MCL, the phase transition leads to the formation of a large number of pores with a diameter between 200 and 400 nm. This may be attributed to the use of agarose as macro-crosslinker that brings about larger and more polydisperse pores, as has been shown previously where the molecular weight of the crosslinker has a large effect on the microporosity in the hydrogel network.[38] Such porous structure allows more efficient water transportation and the formation of smaller pores during phase transitions and thus higher whiteness, similar to previously reported ch-PNIPAm, though based on a different network design.[3]

In highly scattering materials, the optimal size of scattering centers is ≈200–300 nm for visible light.[1,6,7] On the other hand, this size has also been shown to produce a more blue hue in the

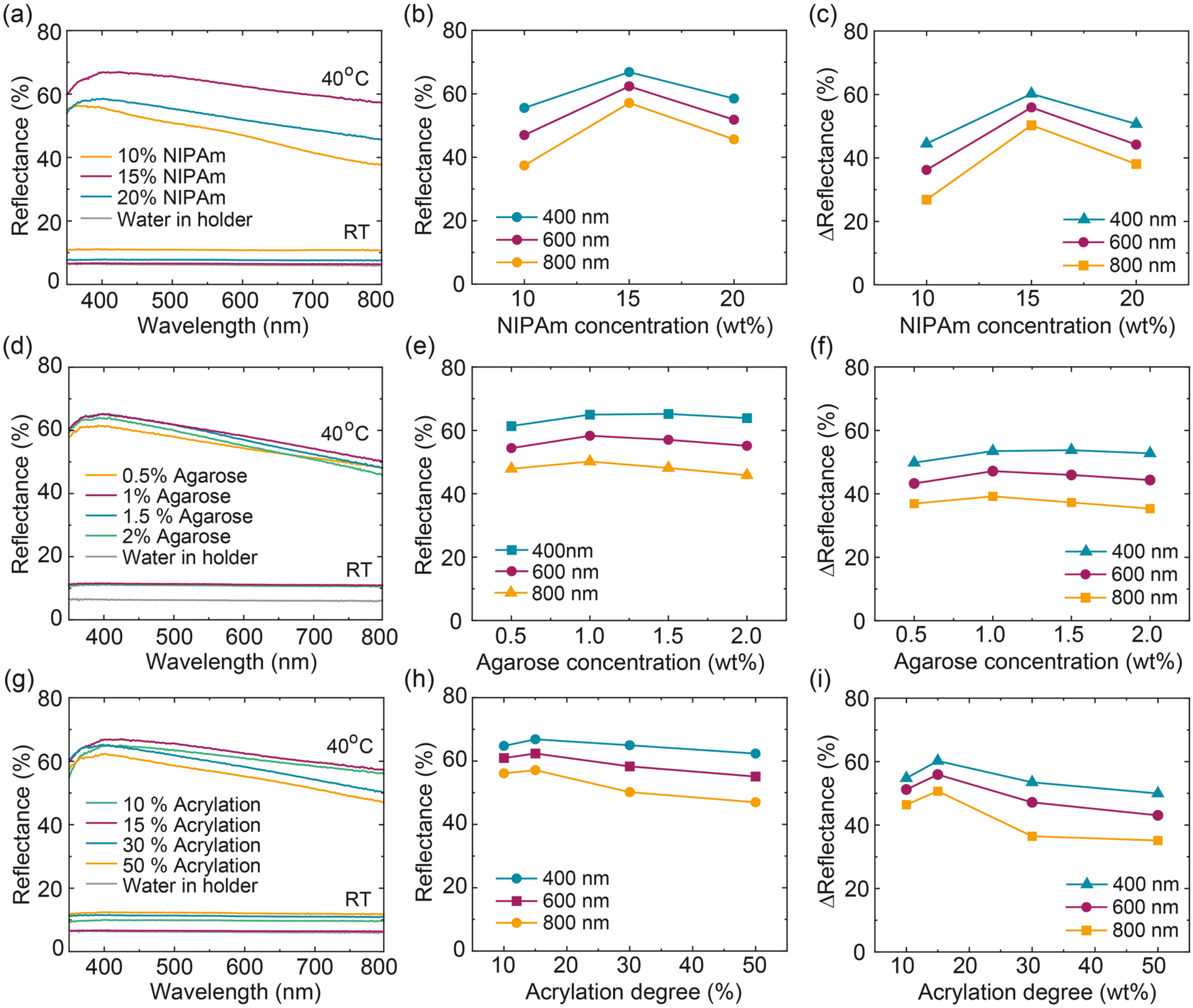

Figure 2. Influence of composition on the switchable reflectance. a) Reflectance spectra at different monomer (NIPAm) concentrations at 40 °C and room temperature (RT). b) Reflectance at 40 °C as a function of monomer content at different wavelengths. c) Reflectance switching (ΔReflectance) between 40 °C and RT as a function of monomer content at different wavelengths. d) Reflectance spectra at different agarose concentrations at 40 °C and RT. Degree of acrylation of agarose was 30%. e) Reflectance at 40 °C as a function of agarose content at different wavelengths. Degree of acrylation of agarose was 30%. f) Reflectance switching (ΔReflectance) between 40 °C and RT as a function of agarose content at different wavelengths. Degree of acrylation of agarose was 30%. g) Reflectance spectra at different acrylation degrees at 40 °C and RT. h) Reflectance at 40 °C as a function of acrylation degree at different wavelengths. i) Reflectance switching between 40 °C and RT as a function of acrylation degree at different wavelengths. Unless otherwise stated, all the hydrogels were measured as 200 µm thick films chemically attached between two glass slides with the monomer solutions containing 15 wt.% NIPAm and 1 wt.% of agarose with the degree of acrylation of 15%.

material, and pores with a diameter between 400 and 600 nm result in a whiter appearance.[17,39] The drawback of the increased pore size is that it leads to a decreased number of scattering centers and thus less efficient scattering.[39] It can be expected that the high scattering properties of the MCL hydrogel above the LSCT are a result of a much larger pore density than that in st. PNIPAm, which allows for more scattering interfaces, combined with the average pore diameters between 200 and 400 nm, closer to the optimal range for visible light.[1,6,7]

2.4. Phase Transition Kinetics

The phase transition kinetics of the MCL hydrogel is studied using photothermal heating to induce fast local temperature jumps and thus phase changes in the hydrogels. The 200 µm thick hydrogel films were prepared with a solution of gold nanoparticles (AuNPs) (diameter 11.0 ± 1.5 nm, Figure S5, Supporting Information) to enable photothermal heating.[3,40] Laser irradiation at 532 nm, close to the absorbance peak of the AuNPs, is used to

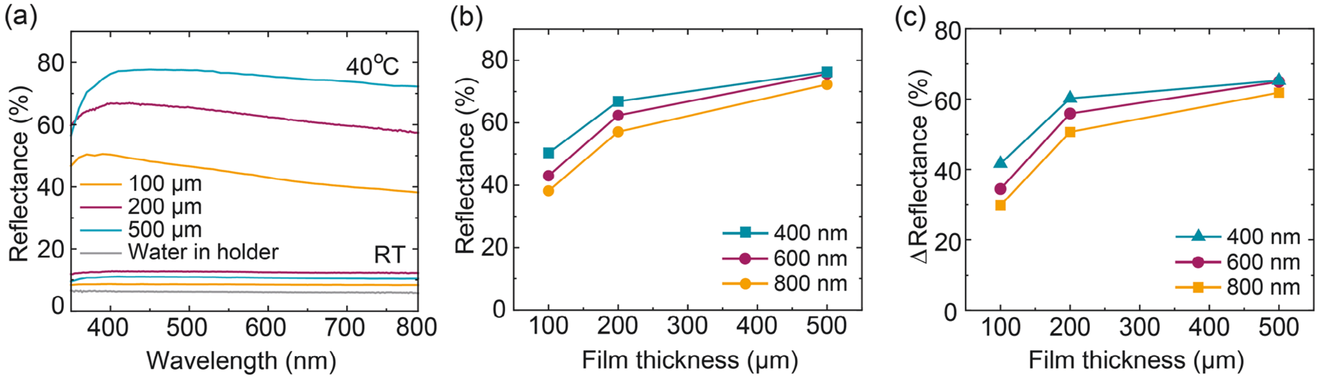

Figure 3. Effect of thickness on the hydrogel reflectance. a) Reflectance spectra at different film thicknesses at 40 °C and RT. b) Reflectance at 40 °C as a function of hydrogel film thickness at different wavelengths. c) Reflectance switching between 40 °C and RT as a function of hydrogel film thickness at different wavelengths. All of the hydrogels were chemically attached between two glass slides with the monomer solutions containing 15 wt.% NIPAm and 1 wt.% of agarose with the acrylation degree of 15%.

induce photothermal heating, and a laser at 635 nm is used to probe the changes in transmittance as illustrated in **Figure** 5a,b. The heating beam is switched on and off and the ratio of the two states is changed to study the effect of the illumination duration and the average laser power on the hydrogel transmittance. The average laser power P_{avg} is defined as:

$$P_{\mathrm{avg}} = P_0 \cdot \frac{t_{\mathrm{on}}}{t_{\mathrm{on}} + t_{\mathrm{off}}} \tag{1}$$

where P_0 is the laser power (400 mW), t_{on} is the duration of the irradiation pulse, and t_{off} is the length of time between the laser pulses.[3] Transmittance of 100% was defined as the transmittance at RT before the start of the experiment.

Figure 5c presents the effect of t_{on} on the transmittance, which ranged from 500 to 30 ms. The average power during the measurement was kept constant at 55 mW. As the pulse duration decreases, the amplitude of the oscillation decreases in the case of the MCL hydrogel. This is due to insufficient heating/cooling duration to reach equilibration of the phase transition for shorter pulses, which leads to less transparency changes. Figure S6a,b (Supporting Information) shows the effect of the t_{on} on the amplitude of transmittance change at different P_{avg}, showing a similar trend of the amplitude increasing at increasing t_{on}.

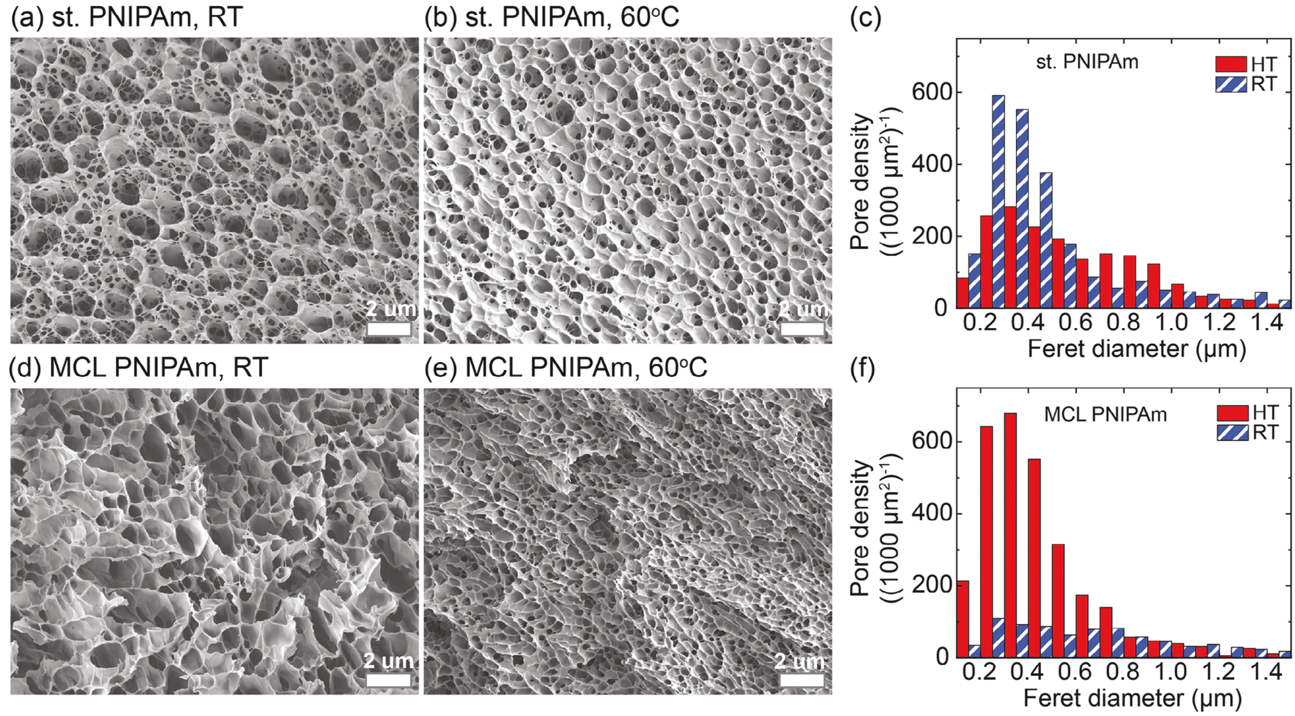

Figure 4. SEM images of freeze-fractured hydrogels. st. PNIPAm at a) RT and b) 60 °C. MCL hydrogel at d) RT and e) 60 °C. All scale bars are 2 µm. Pore densities as a function of the Feret diameter measured from the images of c) st. PNIPAm and f) MCL at 60 °C (HT) and RT.

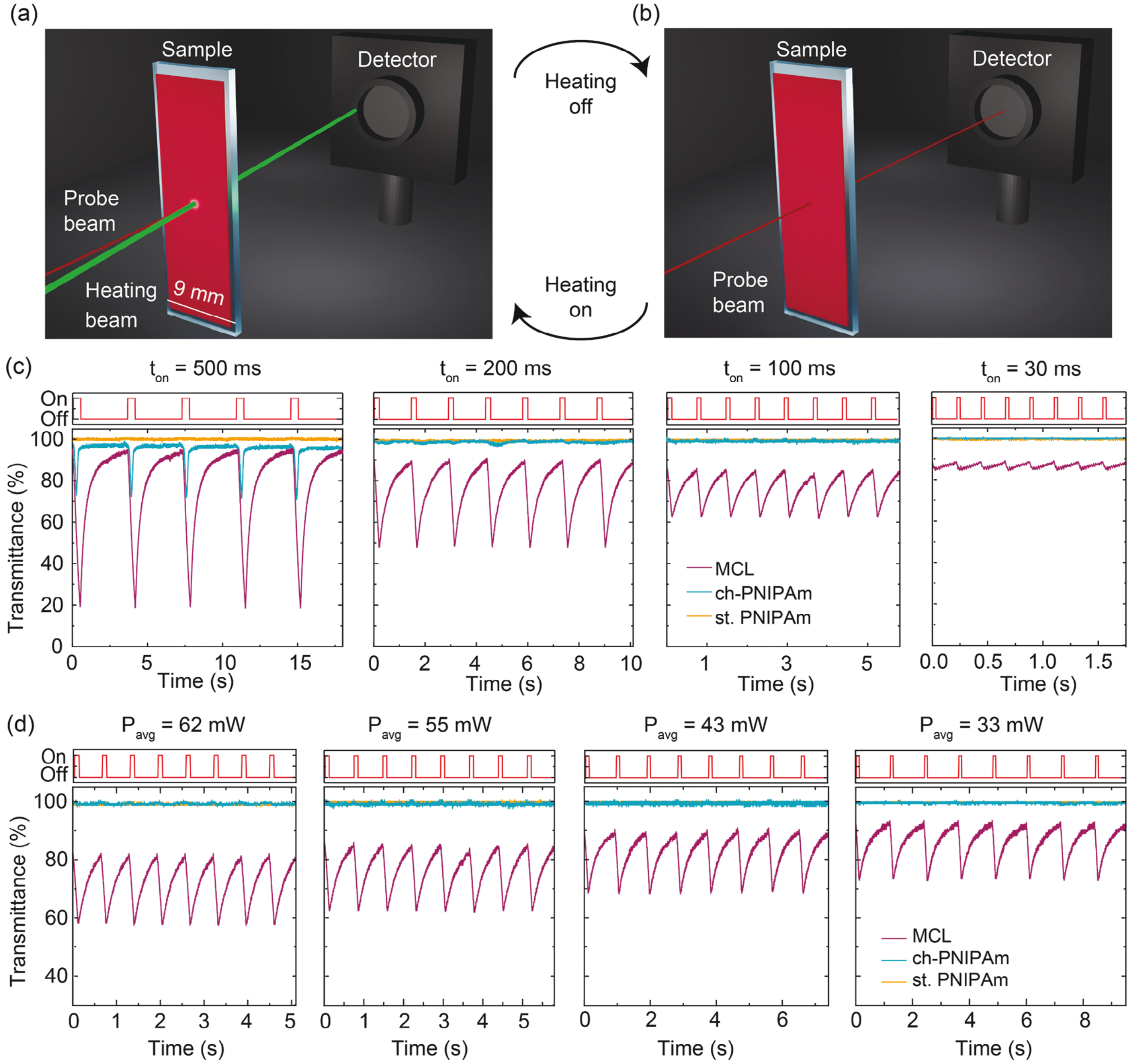

Figure 5. Characterization of phase transition by local photothermal heating. a,b) Illustration of the measurement setup. 200 µm thick hydrogels were prepared with AuNPs, chemically attached to glass on one side, and placed into a water-filled cuvette for the measurement. The heating beam was switched (a) on and (b) off, and the probe beam intensity was measured to determine the transmittance. c) Effect of the heating pulse duration (t_{on}) on the transmittance of MCL hydrogel, ch-PNIPAm, and st. PNIPAm. d) Effect of the average power (P_{avg}) on the transmittance switching of MCL, ch-PNIPAm, and st. PNIPAm. Unless otherwise stated, t_{on} = 100 ms and P_{avg} = 55 mW. Laser power P_0 = 400 mW for all measurements.

In the case of st. PNIPAm and ch-PNIPAm hydrogels, no transmittance changes were observed when t_{on} is below 200 ms. This can be mainly attributed to the lower scattering efficiency in ch-PNIPAm and st. PNIPAm at the small thickness of 200 µm, which leads to little responses. On the other hand, the higher LCST of these two gels (≈35°C)[3] compared to MCL hydrogel (≈31°C, Figure S6a,b, Supporting Information) may also contribute to the lower responsivity as higher temperatures are needed to trigger their phase transition.

Figure 5d shows the effect of P_{avg} at constant t_{on} of 100 ms. While the amplitude remains relatively similar for all MCL hydrogel measurements, the average transmittance increases as P_{avg} decreases. This can be attributed to the increase of average power leading to a higher average temperature and thus a shift of the average transmittance along the LCST curve (Figure S7, Supporting Information). In contrast, ch-PNIPAm and st. PNIPAm did not respond to the 100 ms irradiation at various average powers. Figure S6c,d (Supporting Information) shows the change in

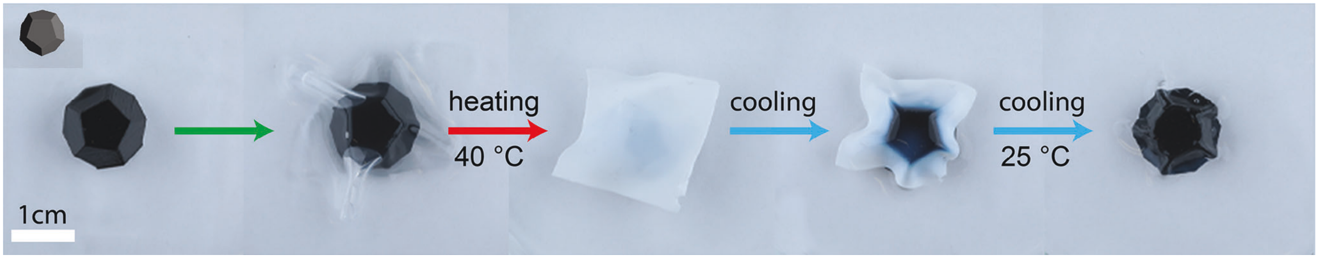

Figure 6. Deformable and thermally switchable MCL hydrogel films. A flat MCL hydrogel film was placed on a 3D-printed black dodecahedron, which underwent heating and cooling cycles showing the deformability of the hydrogel and the switching in the optical appearance of the object. The 0.5 mm-thick MCL hydrogel film consists of 15 wt.% NIPAm and 1 wt.% of acrylated agarose with an acrylation degree of 30%.

transmittance as a function of P_{avg} at different t_{on}. It can be observed that shorter t_{on} results in a smaller amplitude of oscillation, while the P_{avg} does not have a significant effect on the amplitude, especially at $t_{on} < 500$ ms.

To characterize the kinetics of the phase transition, a single-exponential fitting was used to determine the time constant (τ)[3,40–42] of both the heating and cooling processes of MCL and ch-PNIPAm hydrogels as shown in Figure S8 (Supporting Information). For the heating process, the τ for the MCL hydrogel is 410 ms and for the ch-PNIPAm 490 ms, indicating similar transition kinetics. On the other hand, for the cooling process the corresponding times are 440 and 85 ms, respectively, where the ch-PNIPAm had faster kinetics. This excludes the effect of kinetics in the enhanced responsivity of MCL hydrogels shown in Figure 5.

To summarize, t_{on} strongly affects the oscillation amplitude, while P_{avg} mainly changes the average transmittance with little effect on the amplitude. There is a significantly larger change in the transmittance in the case of the MCL hydrogel compared to the others, which can be attributed to the enhanced light scattering capability as well as lower phase transition temperature in the MCL hydrogels.

2.5. Deformable and Optically Switchable MCL Films

We demonstrate the application potential of the MCL hydrogels as a deformable and optically switchable film in **Figure 6**, where the MCL hydrogel film was placed on top of a black plastic dodecahedron. The hydrogel film deforms easily to accommodate the shape of the dodecahedron. Upon heating above 40 °C, the hydrogel film became highly scattering and conceals the shape of the dodecahedron behind the hydrogel. Upon cooling to rRT, the top surface of the hydrogel first transitions back to transparent state, which partially reveals the dodecahedron. Upon complete cooling of the hydrogel, the dodecahedron became fully visible with the hydrogel film closely attached due to shrinking of the hydrogel during the heating process. The hydrogel film's high deformability and switchability of whiteness makes it a suitable candidate for applications involving visual camouflage of irregular objects or displays with controllable transparency.

3. Conclusion

This work introduces a method of using chemically modified agarose to crosslink temperature-responsive PNIPAm, resulting in a macro-crosslinked hydrogel network capable of switching between highly transparent and scattering states depending on the temperature. The system exhibits superior visible light scattering capability above the LCST (≈31 °C) compared to previously reported hydrogel systems. At 40 °C, the reflectance of the MCL hydrogel (47%) is four times higher than for standard PNIPAm at 800 nm at a thickness of 200 µm. The reflectance at 600 nm is above 40% at a thickness of 100 µm, i.e., only half of the thickness of channeled PNIPAm to reach the same reflectance. Upon local photothermal heating, the MCL hydrogel can respond to laser pulses as short as 30 ms, while st. or ch-PNIPAm does not respond to pulses below 200 ms under the same conditions. The hydrogel composition is optimized to provide high scattering, and the resulting pore structure is optimal for reflecting the visible light wavelengths with an average pore diameter of 350 nm and a high density of scattering interfaces. This allows the system to be used in applications such as controllable reflective displays, flexible optical switches, and smart windows.

4. Experimental Section

Materials: *N*-isopropylacrylamide (99%) was purchased from Merck and recrystallized from *n*-hexane (≥ 97%, Sigma–Aldrich). *N,N′*-Methylenebisacrylamide (≥99.5%, BIS), acrylamide (≥99%), agaroses (A1 = Ultra-low Gelling Temperature, A5030, A3 = low gelling temperature, A4018, and A5 = low EEO, A0576), gold(III) chloride trihydrate ($HAuCl_4{\cdot}3H_2O$, >99.9% trace metals basis), sodium citrate tribasic dihydrate (BioUltra, 99.5%), poly(ethylene glycol) methyl ether thiol (PEG-SH, $M_n = 2000$), 3-(trimethoxysilyl)propyl acrylate (≥92%), *N,N*-dimethylacetamide (DMAc, 99%), acryloyl chloride (97%), dimethyl sulfoxide-d6 (99.9 atom.% D), acetone (99.5%) and 2-hydroxy- 4′-(2-hydroxyethoxy)-2-methylpropiophenone (photoinitiator, Irgacure 2959, 98%) were purchased from Sigma–Aldrich. Ethanol (99.5%) was purchased from Altia Oyj, Finland. Deionized water (18.2 MΩ; DirectQ 3 UV; Millipore) was used in all experiments.

Preparation and Modification of Gold Nanoparticles: Gold nanoparticles (AuNPs) were prepared using citrate reduction method.[43] Aqueous solution of $HAuCl_4 \cdot 3\,H_2O$ (100 mL, 0.01 wt.%) was brought to boil under vigorous stirring and trisodium citrate (2 mL, 1.00 wt.%) was quickly injected in. The solution was refluxed for 10 min under constant stirring. The AuNPs were stabilized with poly(ethylene glycol) (PEG) by mixing PEG-SH-ethanol solution (8 mL, 5 mg mL^{-1}) with the AuNPs solution (85 mL). The solution was stirred overnight on an orbital shaker, and the modified AuNPs were washed by centrifugation (16 000 g for 25 min) and re-dilution in water for three times. This resulted in a concentrated stock solution (0.88 mL) of PEG-AuNPs that was used in sample preparation for studying the hydrogel kinetics. The AuNPs were analyzed using transmission electron microscopy (Tecnai 12, FEI, USA).

Silanization of Glass: Glass slides (Corning, Merck) were cut to 9 mm wide pieces and cleaned by sonication in deionized water for 10 min and plasma treatment (Pico, Diener Electronic GmbH, Germany) for 5 min. The glass slides were placed to a desiccator along with 3-(trimethoxysilyl)propyl acrylate (100 µL), and evacuated to a vacuum of 8×10^{-2} Pa overnight. The remaining silane was taken out after overnight storage and the desiccator was evacuated for 2 h at 1×10^{-3} Pa. The functionalized glass was stored in a fridge.

Acrylation of Agarose: The agarose was modified following a previous protocol.[44] Agarose (1.0 g) was dissolved in DMAc (25 mL) at 100 °C. The solution was cooled to 0 °C using an ice–water bath. Acryloyl chloride (38 µL for 15% theoretical acrylation degree) was dissolved in DMAc (1 mL) and added to the agarose solution slowly while stirring. The stirring was continued at 0 °C for 1 h and at RT for 4 h. The acrylated agarose was precipitated, washed with acetone, and dried under vacuum.

Hydrogel Preparation: The MCL hydrogel films were prepared by first preparing a 2.5 wt.% solution of the acrylated agarose A3 by heating and vortexing. The solution was bubbled with nitrogen before transferring to a glove box. NIPAm (35 mg) and initiator (0.69 mg) were weighed into a vial, and after transferring to the glove box, deionized water (105 µL) and agarose solution (93 µL) were used to dissolve them to produce a solution with 15 wt.% of NIPAm, 1 mol.% of initiator, and 1 wt.% of agarose. The solution was injected to a holder with two glass slides separated by a parafilm spacer and polymerized at 45 °C for 40 min using a UV-lamp (Spectroline ENF-260, Spectronics Corporation, USA).

ch-PNIPAm films were prepared by dissolving agarose A1 (3.51 mg) into water (1.04 mL) by heating and vortexing. NIPAm (20.7 mg) and initiator (41 mg) were weighed into a vial, and agarose solution (183 µL) was used to dissolve them to produce a monomer solution with 10 wt.% NIPAm, 1 mol.% initiator and 0.3 wt.% agarose. Crosslinker BIS was added (1.83 µL, 100 mM) to achieve a crosslinking density of 0.1 mol.%. The solution was bubbled with nitrogen for 10 min, after which it was injected to holders consisting of two glass slides held together with a parafilm spacer under nitrogen. The vials were placed into a fridge at 4 °C for 30 min for the agarose to form a gel, and then polymerized in a UV-reactor (8 × 14 W lamps, 350 nm, Rayonet, USA) for 30 min. st. PNIPAm was prepared using the same procedure but using water instead of agarose solution to dissolve the monomer. The hydrogels were washed in water by placing the vial into a water bath at 50 °C for 10 min, replacing the water in the vial with RT water to swell the samples for 30 min, and repeating twice.

UV–vis–NIR Spectroscopy: The spectra between 300 and 2000 nm were measured with a Cary 5000 (Agilent, USA) spectrophotometer. Total reflectance was measured using an integrating sphere (DRA 2500, Agilent) and sample temperature was controlled with a TMS94 temperature controller (Linkam, UK). The transmittance was measured at 500 nm using a dual cell Peltier sample holder. The LCST was defined as the point at which the transmittance was 50%. The CIELAB coordinates were determined using the Scan program (version 6.2.0.1588) of the instrument.

SEM Characterization: Hydrogel pieces were cut and frozen in liquid nitrogen from RT or 60 °C. After freeze-fracturing, the samples were placed into a round bottom flask, which was evacuated to a pressure of 1×10^{-3} mbar, and the temperature was increased slowly to RT. The freeze-dried samples were attached to SEM stubs using carbon tape and sputter coated with 8 nm of Pt/Pd using EM ACE600 sputter coater (Leica, Germany). SEM Sigma VP (Zeiss, Germany) was used for imaging.

Porosity Analysis: The SEM images were converted into binary ones using the Threshold function of ImageJ (V 1.53t). The resulting images were analyzed using the Analyze particles function to calculate the Feret diameter of the pores, which refers to the caliper diameter, or the maximum distance between two points on the pore edge. Pores smaller than 100 nm were excluded from the analysis and over 300 pores were analyzed for each sample. The pore density was calculated by dividing the number of pores by the image area.

Photothermal Kinetics Measurement: Hydrogels were prepared using PEG-AuNPs solution instead of water, to an optical density of 0.4 at a thickness of 200 µm. The hydrogel was chemically attached to a glass slide on one side. The sample was placed into a glass cuvette (100-OS, Hellma Analytics, Germany) with deionized water to prevent hydrogel drying. The cuvette was placed in between a mechanical shutter (SH1, Thorlabs, USA) and a photometer (PDA100A-EC, Thorlabs, USA) connected to an oscilloscope (WaveSurfer 3074, Teledyne LeCroy, USA), which was used to record the transmittance. The heating laser beam (MGL-F-532-2 W, Roithner Lasertechnic, Austria) had a wavelength of 532 nm, and the probe laser (MDL-D-635-1 W, Roithner Lasertechnic, Austria) 635 nm. The probe beam was positioned to the middle of the heating beam, only the probe beam reached the filter and only the heating beam was controlled by the shutter and the probe beam was constantly on. Due to the low absorbance of the AuNPs at 635 nm, the heating effect was negligible. The sample was repositioned between every measurement so that the beam would hit a new spot to ensure consistency of the results. The laser beam power was measured using a LabMax-TO power meter (Coherent, USA). The 100% transmittance was defined as the transmittance through the sample at RT, and thus does not take into account the light scattered by the cuvette or the sample. Both 0% and 100% transmittance were measured for calibration before each measurement by blocking the probe beam. The exponential fitting was done using function ExpDecay1 in OriginPro (Version 2023, OriginLab Corporation, USA).[3]

Video and Photo Capture: Canon 5D Mark IV with a Sigma 105 mm 1:2.8 DG macro HSM objective was used to capture the photos.

3D Printing of Dodecahedron: The regular dodecahedron model was constructed in SOLIDWORKS (2021, Dassault Systèmes SOLIDWORKS Corp.) and sliced by Ultimaker Cura software (5.2.1). After scaling to the desired size, the model was printed by Ultimaker S3 (Ultimaker B.V.) with a layer height of 0.1 mm. The filament material and extruder size were black tough polylactic acid and 0.25 mm, respectively.

Preparation of MCL Hydrogel Film: Two pieces of glass (5 cm × 5 cm) were assembled with a parafilm spacer of 500 µm thickness (Parafilm M, Bemis) to form a glass mold. Subsequently, 1.98 mg photo-initiator, 100 mg of PNIPAm, 300 µL of deionized water, and 267 µL of 2.5 wt.% ac-agarose (DS, 30) were mixed to create a homogenous solution, which was bubbled by nitrogen to eliminate oxygen for 1 min and then transferred into the glass mold. Following this, the mixture was cooled down in the 7 °C refrigerator for 30 min until the gelation of ac-agarose occurred. Lastly, the precursor was polymerized in a UV chamber (8 × 14 W lamps, 350 nm, Rayonet, USA) at RT for 2 h.

Supporting Information

Supporting Information is available from the Wiley Online Library or from the author.

Acknowledgements

A.E. and S.H. contributed equally to this work. The authors acknowledge the provision of facilities and technical support by Aalto University at OtaNano - Nanomicroscopy Center (Aalto-NMC) and funding from Academy of Finland (Postdoctoral Researcher No. 331015 to H.Zhang, Center of Excellence in Life-Inspired Hybrid Materials–LIBER No. 346108 to O.I. and No. 346107 to A.P., and Flagship PREIN No. 320165 to A.P.), China Scholarship Council (No. 202207960015 to Y.F.), and the European Research Council (Advanced Grant DRIVEN No. 742829 to O.I., Consolidator Grant MULTIMODAL No. 101045223 to A.P., and Starting Grant ONLINE No. 101076207 to H.Zeng).

Conflict of Interest

The authors declare no conflict of interest.

Data Availability Statement

The data that support the findings of this study are available from the corresponding author upon reasonable request.

Keywords

hydrogels, LCST, macro-crosslinkers, reflectance, switching, whiteness

Received: October 3, 2023
Revised: December 10, 2023
Published online: December 31, 2023

[1] J. Syurik, R. H. Siddique, A. Dollmann, G. Gomard, M. Schneider, M. Worgull, G. Wiegand, H. Hölscher, *Sci. Rep.* **2017**, *7*, 46637.
[2] A. Weir, P. Westerhoff, L. Fabricius, K. Hristovski, N. Von Goetz, *Environ. Sci. Technol.* **2012**, *46*, 2242.
[3] A. Eklund, H. Zhang, H. Zeng, A. Priimagi, O. Ikkala, *Adv. Funct. Mater.* **2020**, *30*, 2000754.
[4] T. Li, Y. Zhai, S. He, W. Gan, Z. Wei, M. Heidarinejad, D. Dalgo, R. Mi, X. Zhao, J. Song, J. Dai, C. Chen, A. Aili, A. Vellore, A. Martini, R. Yang, J. Srebric, X. Yin, L. Hu, *Science* **2019**, *364*, 760.
[5] Y. Zhou, X. Dong, Y. Mi, F. Fan, Q. Xu, H. Zhao, S. Wang, Y. Long, *J. Mater. Chem. A* **2020**, *8*, 10007.
[6] P. Vukusic, B. Hallam, J. Noyes, *Science* **2007**, *315*, 348.
[7] B. Yu, Z. Huang, D. Fang, S. Yu, T. Fu, Y. Tang, Z. Li, *Adv. Mater. Interfaces* **2022**, *9*, 2101485.
[8] G. Jacucci, L. Schertel, Y. Zhang, H. Yang, S. Vignolini, *Adv. Mater.* **2021**, *33*, 2001215.
[9] B. D. Wilts, X. Sheng, M. Holler, A. Diaz, M. Guizar-Sicairos, J. Raabe, R. Hoppe, S.-H. Liu, R. Langford, O. D. Onelli, D. Chen, S. Torquato, U. Steiner, C. G. Schroer, S. Vignolini, A. Sepe, *Adv. Mater.* **2018**, *30*, 1702057.
[10] D. S. Wiersma, *Nat. Photonics* **2013**, *7*, 188.
[11] L. Cortese, L. Pattelli, F. Utel, S. Vignolini, M. Burresi, D. S. Wiersma, *Adv. Opt. Mater.* **2015**, *3*, 1337.
[12] J. S. Haataja, G. Jacucci, T. G. Parton, L. Schertel, S. Vignolini, *Commun. Phys.* **2023**, *6*, 137.
[13] M. S. Toivonen, O. D. Onelli, G. Jacucci, V. Lovikka, O. J. Rojas, O. Ikkala, S. Vignolini, *Adv. Mater.* **2018**, *30*, 1704050.
[14] M. Burresi, L. Cortese, L. Pattelli, M. Kolle, P. Vukusic, D. S. Wiersma, U. Steiner, S. Vignolini, *Sci. Rep.* **2014**, *4*, 6075.
[15] A. J. Parnell, A. L. Washington, O. O. Mykhaylyk, C. J. Hill, A. Bianco, S. L. Burg, A. J. C. Dennison, M. Snape, A. J. Cadby, A. Smith, S. Prevost, D. M. Whittaker, R. A. L. Jones, J. P. A. Fairclough, A. R. Parker, *Sci. Rep.* **2015**, *5*, 18317.
[16] J. Syurik, G. Jacucci, O. D. Onelli, H. Hölscher, S. Vignolini, *Adv. Funct. Mater.* **2018**, *28*, 1706901.
[17] S. L. Burg, A. Washington, D. M. Coles, A. Bianco, D. Mcloughlin, O. O. Mykhaylyk, J. Villanova, A. J. C. Dennison, C. J. Hill, P. Vukusic, S. Doak, S. J. Martin, M. Hutchings, S. R. Parnell, C. Vasilev, N. Clarke, A. J. Ryan, W. Furnass, M. Croucher, R. M. Dalgliesh, S. Prevost, R. Dattani, A. Parker, R. A. L. Jones, J. P. A. Fairclough, A. J. Parnell, *Commun. Chem.* **2019**, *2*, 100.
[18] V. A. Maiorov, *Opt. Spectrosc.* **2020**, *128*, 367.
[19] K. Connelly, Y. Wu, X. Ma, Y. Lei, *Energies* **2017**, *10*, 1889.
[20] K. Connelly, Y. Wu, J. Chen, Y. Lei, *Appl. Energy* **2016**, *182*, 331.
[21] A. Nakamura, R. Ogai, K. Murakami, *Sol. Energy Mater. Sol. Cells* **2021**, *232*, 111348.
[22] X. Liu, Y. Wu, *Appl. Energy* **2021**, *303*, 117521.
[23] Y. Ming, Y. Sun, X. Liu, X. Liu, Y. Wu, *Energy Convers. Manag. X* **2022**, *16*, 100315.
[24] Y. Zhou, S. Wang, J. Peng, Y. Tan, C. Li, F. Y. C. Boey, Y. Long, *Joule* **2020**, *4*, 2458.
[25] Y. Ding, Y. Duan, F. Yang, Y. Xiong, S. Guo, *Chem. Eng. J.* **2023**, *460*, 141572.
[26] A. Halperin, M. Kröger, F. M. Winnik, *Angew. Chem. Int. Ed.* **2015**, *54*, 15342.
[27] H. Zhu, L. Wang, *Sol. Energy Mater. Sol. Cells* **2019**, *202*, 110109.
[28] G. Wei, D. Yang, T. Zhang, X. Yue, F. Qiu, *Sol. Energy Mater. Sol. Cells* **2020**, *206*, 110336.
[29] M. Wu, Y. Shi, R. Li, P. Wang, *ACS Appl. Mater. Interfaces* **2018**, *10*, 39819.
[30] X.-H. Li, C. Liu, S.-P. Feng, N. X. Fang, *Joule* **2019**, *3*, 290.
[31] T.-G. La, X. Li, A. Kumar, Y. Fu, S. Yang, H.-J. Chung, *ACS Appl. Mater. Interfaces* **2017**, *9*, 33100.
[32] H. Zhang, H. Zeng, A. Eklund, H. Guo, A. Priimagi, O. Ikkala, *Nat. Nanotechnol.* **2022**, *17*, 1303.
[33] F. A. Plamper, W. Richtering, *Acc. Chem. Res.* **2017**, *50*, 131.
[34] X. S. Wu, A. S. Hoffman, P. Yager, *J. Polym. Sci. Part A Polym. Chem.* **1992**, *30*, 2121.
[35] G. Jacucci, J. Bertolotti, S. Vignolini, *Adv. Opt. Mater.* **2019**, *7*, 1900980.
[36] X. Cai, Y. Wang, Y. Luo, J. Xu, L. Zhao, Y. Lin, Y. Ning, J. Wang, L. Gao, D. Li, *ACS Appl. Mater. Interfaces* **2022**, *14*, 27222.
[37] A. Eklund, O. Ikkala, H. Zhang, *Adv. Funct. Mater.* **2023**. https://doi.org/10.1002/adfm.202214091
[38] S. Pruksawan, J. W. R. Lim, Y. L. Lee, Z. Lin, H. L. Chee, Y. T. Chong, H. Chi, F. Wang, *Commun. Mater.* **2023**, *4*, 75.
[39] B. T. Hallam, A. G. Hiorns, P. Vukusic, *Appl. Opt.* **2009**, *48*, 3243.
[40] J. Zhao, H. Su, G. E. Vansuch, Z. Liu, K. Salaita, R. B. Dyer, *ACS Nano* **2019**, *13*, 515.
[41] J. Wang, D. Gan, L. A. Lyon, M. A. El-Sayed, *J. Am. Chem. Soc.* **2001**, *123*, 11284.
[42] E. Sato Matsuo, T. Tanaka, *J. Chem. Phys.* **1988**, *89*, 1695.
[43] G. Frens, *Nat. Phys. Sci.* **1973**, *241*, 20.
[44] S. Hu, Y. Fang, C. Liang, M. Turunen, O. Ikkala, H. Zhang, *Nat. Commun.* **2023**, *14*, 3717.